Available online at www.sciencedirect.com
ScienceDirect
Journal of the European Ceramic Society 28 (2008) 1909–1916
www.elsevier.com/locate/jeurceramsoc

Microstructure and mechanical properties of hot-pressing chromium carbide/alumina nanocomposite prepared by MOCVD in fluidized bed

Sheng-Chang Wang [a,*], Yuan-Liang Chin [b], Jow-Lay Huang [b]

[a] Department of Mechanical Engineering, Southern Taiwan University, No. 1, Nan-Tai St., Yungkang City, Tainan County 710, Taiwan
[b] Department of Materials Science and Engineering, National Cheng Kung University, No. 1, University Road, Tainan 701, Taiwan

Received 4 June 2007; received in revised form 7 December 2007; accepted 16 December 2007
Available online 3 March 2008

Abstract

Nanocomposites of Cr_3C_2/Al_2O_3 were prepared by metal-organic chemical vapor deposition (MOCVD) method in a fluidized bed and sintered under hot-pressed condition at 1500 °C for1 h. The TEM microstructure showed that the Al_2O_3 matrix contained both intragranular and intergranular phase of Cr_3C_2. The hot-pressed Cr_3C_2/Al_2O_3 nanocomposites possessed better mechanical performance as regard to bending strength and fracture toughness in comparison to the monolithic Al_2O_3. The phenomenal change of the fracture mode from intergranular fracture of monolithic Al_2O_3 to transgranular fracture of nanocomposites is attributed to the enhancement of the residual stress and formation of a solid solution, eventually improving the strength of the Cr_3C_2/Al_2O_3 nanocomposite. Furthermore, it has been deciphered that the toughening mechanisms of the nanocomposites contribute to the crack deflection and the residual stress.

Keywords: Cr_3C_2/Al_2O_3; Nanocomposite; MOCVD; Residual stress; Strengthening mechanism

1. Introduction

Alumina (Al_2O_3) is available from abundant deposits and is a low-cost ceramic material. It is widely used in mechanical and electronic applications due to its good thermal resistance, chemical stability, wear resistance, and insulation. But applications of monolithic Al_2O_3 are limited by its intrinsic mechanical properties, such as poor toughness, low strength and reliability due to abnormal grain growth during the sintering, as well as brittle fracture behavior and the low crack tolerance due to the ionic and covalent bonding. Therefore, improvement of the fracture toughness and strength of Al_2O_3 is an important and challenging area in the realm of structural ceramics.

Over the past several decades, there have been consistent efforts on improving the strength as well as the toughness of alumina, by the use of nanocomposites.[1–4] The incorporation of hard particulate reinforcement has been shown to be an easy, safe and economically viable toughening technique for alumina ceramics. Depending on the Young's modulus and thermal coefficient values, different kinds of carbides and oxides are utilized as the reinforcement phases in Al_2O_3 matrix to improve its mechanical properties. For example, SiC[1] and Si_3N_4[5] are utilized since their Young's modulus and thermal expansion coefficients are smaller than the Al_2O_3 matrix. In contrast, ZrO_2[6] and MgO[1] are added because of their higher Young's modulus and thermal expansion coefficient.

Utilization of these additives has resulted in improved mechanical properties and enhanced temperature oxidation resistance of chromium carbide/alumina composites.[3–5] In addition, Cr_3C_2 is a material with high electrical conductivity and corrosion resistant at high temperatures. The Cr_3C_2/ceramic composite has potential applications for electrical discharge machining (EDM).[7] Furthermore, the strengthening effect by a solid solution of Cr_2O_3 in the Al_2O_3 matrix is a significant issue for structural ceramics.

Various methods such as gas condensation,[8] laser induced pyrolysis,[9] sol–gel,[10,11] microwave plasma,[12] and gamma radiation[13] synthesis have been utilized to synthesize nanophase Cr_2O_3 or nanocomposites. The a priori condition for formation of nanocomposites with enhanced mechanical properties is the homogeneous dispersion of the second phase and incorporation

* Corresponding author.
E-mail address: scwang@mail.stut.edu.tw (S.-C. Wang).

0955-2219/$ – see front matter © 2008 Elsevier Ltd. All rights reserved.
doi:10.1016/j.jeurceramsoc.2007.12.027

Table 1
Apparent density, porosity and the second phase contents of Cr_3C_2/Al_2O_3 nanocomposites with different deposition time

Deposition time (h)	Apparent density (g/cm^3)	Apparent porosity (%)	Cr_3C_2 contents (vol%)
0 (monolithic Al_2O_3)	3.94	0.8	0
0.5	4.01	0.98	2.2
1	4.03	2.17	5.2
1.5	4.10	1.16	6.2
2	4.11	1.26	6.8

of nanocomposites with optimum density, without notable grain growth. Therefore, in this study, metal-organic chemical vapor deposition conducted in a fluidized powder reactor was used to prepare the Cr_3C_2/Al_2O_3 nanocomposite. The precursor of chromium oxide was deposited on the surface of Al_2O_3 particle in vapor phase. Then, the chromium oxide was carbonized and densified at the same time by hot-pressed sintering. The second phase was coated on the matrix gradually, which reduces to the molecular scale size of the second phase. This hot-pressed sintered composite, can prevent grain growth during the final stage of the densification and produce a nanocomposite with uniform second phase distribution. This was considered the most appropriate combination method to obtain final sintered samples with uniformly dispersed second phase and high density, in proximity to the theoretical maximum.

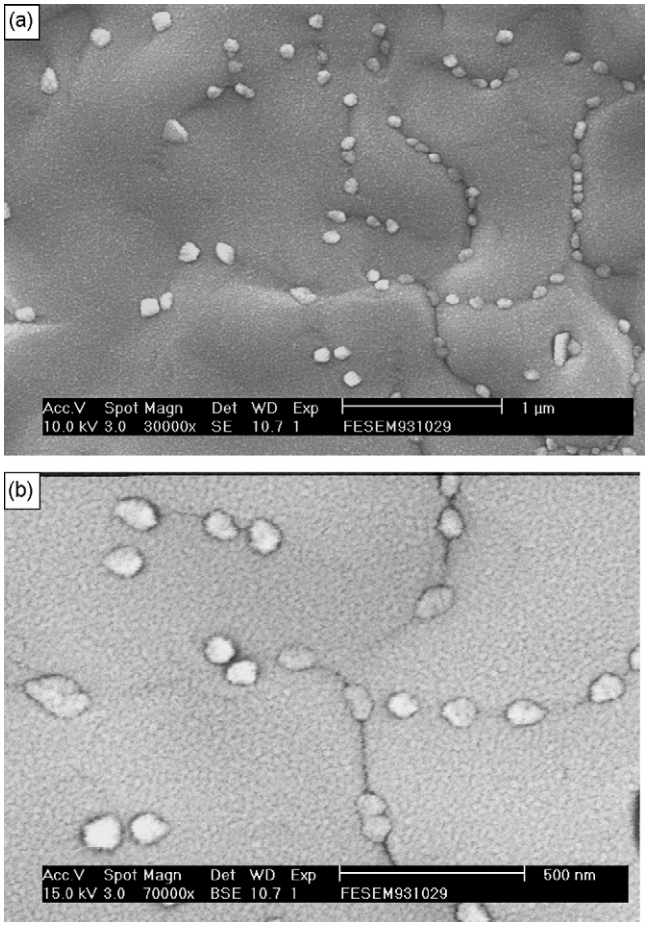

Fig. 1. FE-SEM micrographs of chromium carbide/alumina nanocomposites prepared by MOCVD method for 2 h and hot-pressed at 1500 °C for 1 h in vacuum, (a) SE image and (b) BSE image.

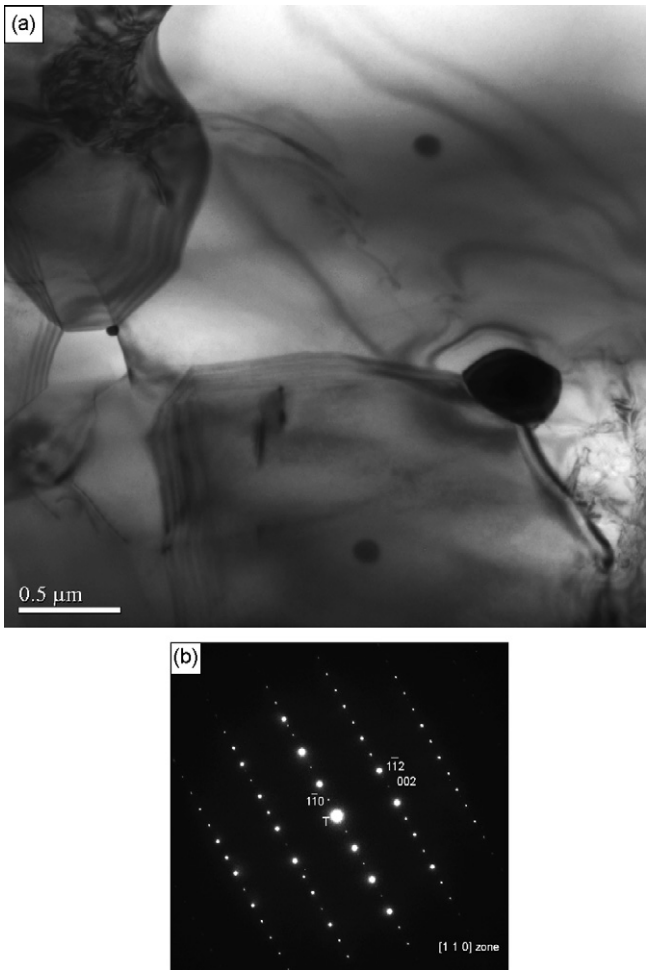

Fig. 2. TEM micrographs of chromium carbide/alumina nanocomposites prepared by MOCVD method for 2 h and hot-pressed at 1500 °C for 1 h in vacuum, (a) bright field image; (b) SADP of B in (a).

2. Experimental procedure

The starting composite powders were fabricated by metal-organic chemical vapor deposition (MOCVD) method in a fluidized bed.[14] The precursor comprising of metal-organic chromium hexacarbonyl ($Cr(CO)_6$, 99% Strem Chemicals Co., USA) was initially heated for evaporation at 85 °C. Inert He gas was used as the carrier gas for transporting these precursor vapors, into the reaction chamber for coating on the fluidized alumina powder (α-Al_2O_3, 99.9%, A16SG, Alcoa, USA). The pressure of reaction chamber was controlled at 10 torr, which can fluidize the Al_2O_3 powder uniformly. The reaction temperature was kept at 400 °C and the deposition times were 0.5, 1, 1.5, and 2 h. The as-deposited powder was processed for 1 h with vibration ball-milling using zirconia balls for reducing the agglomerate and thoroughly dispersing the second phase on the Al_2O_3 powder surface. The powder was sieved through a 200-mesh screen and hot-pressed in vacuum under a pressure of 25 MPa at 1500 °C for 1 h in a graphite die.

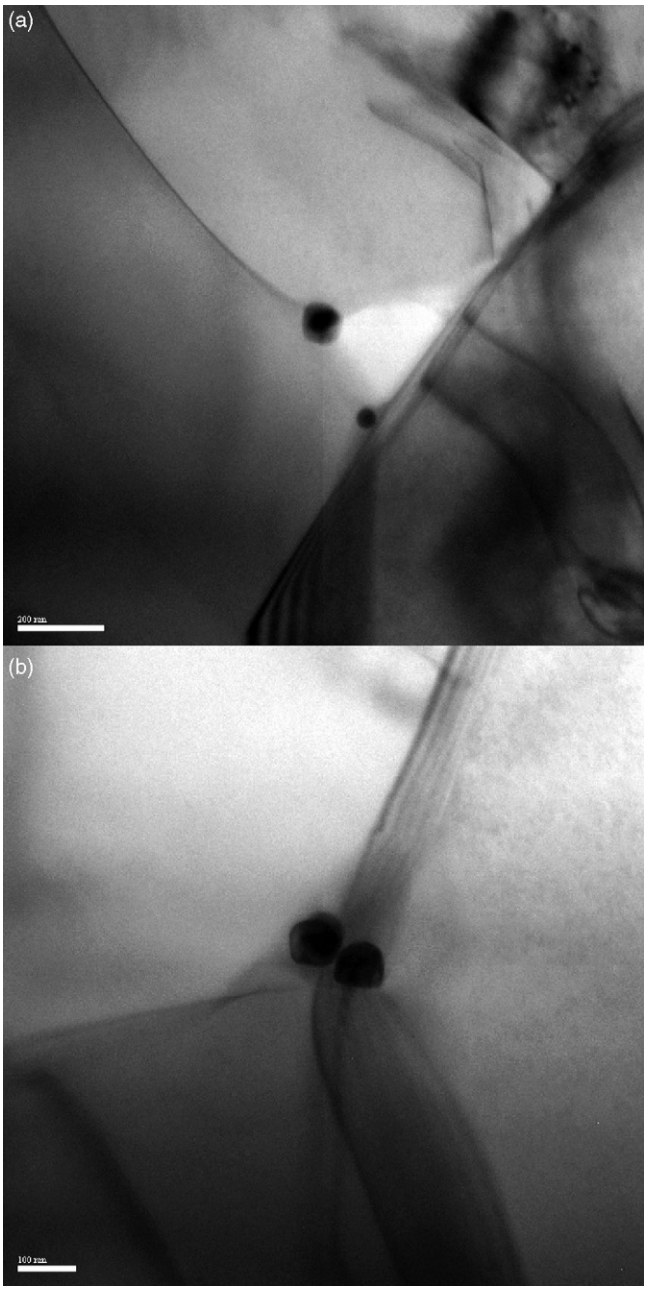

Fig. 3. TEM micrographs of chromium carbide/alumina nanocomposites prepared by MOCVD method for 2 h and hot-pressed at 1500 °C for 1 h in vacuum, (a) nano-sized inclusion in triple junction; (b) nano-sized inclusion in multiple junction.

The sintering density of the composite was measured by the Archimedes method. The porosity was measured by mercury porosimetry (Quantachrome PoreMaster 60, FL, USA). X-ray diffractomerty (Regaku D/max-II B, Japan) was used to identify the phases in the powders and bulk composite. The microstructure was observed by field emission scanning electron microscopy (FESEM, Philips XL-40, Netherlands) and analytical transmission electron microscopy (AEM, FEI, Tecnai G2 F20, Netherlands) equipped with high angle annular dark field (HAADF) detector. XPS (X-ray photoelectron spectroscopy, VG Scientific 210, England) was used to characterize the coating phases by determination of binding energy.

The sintered specimens were machined and polished with a diamond wheel. The final dimensions of the specimens were 4 mm × 3 mm × 45 mm. The four-point bending test was used to measure the fracture strength of all materials. The samples for the bending test were prepared as per the ASTM C1161 standard method by using an Instron 8511 Materials Testing System (Canton, MA, USA). The widths of upper and lower span were 20 and 40 mm, respectively. Hardness was measured by Vickers hardness tester (AKASHI AVK-A, Japan). Fracture toughness was measured by the indentation fracture method.[15] Each data point for fracture strength or toughness was measured for at least 5 samples.

The second phase content was estimated by using the rule of mixture. This implicitly assumes that the apparent density of the composite is in the vicinity of optimum density, and the additional density of the composites above that of monolithic Al_2O_3 are attributed to the addition of the second phases.

$$\rho_{\text{comp}} = \rho_{\text{m}} V_{\text{m}} + \rho_{\text{s}} V_{\text{s}} \tag{1}$$

where the ρ represents the density and V represents the volume percentage and $V_{\text{m}} + V_{\text{s}} = 1$. In additional, for suffixes, comp indicates the properties of composite, s indicates the second phase (Cr_3C_2), and m indicates the properties of the matrix (Al_2O_3). The theoretical density of Al_2O_3 and Cr_3C_2 are 3.98 g/cm^3 and 6.66 g g/cm^3 [16], respectively. Each result is the average of at least 5 repetitions.

The residual stress of the composite was measured by X-ray diffractometer (Siemens D-5000, Germany) using the $\sin^2 \psi$ method.[17] The residual stress was calculated based on the displacement of plane spacing for different orientations of X-ray beams relative to the specimen, where ψ is the angle between the diffraction plane normal and specimen surface normal. In this study, several orientations including 0°, 18.43°, 26.56°, 33.21°, 39.23°, 45° were chosen and the residual stress was calculated by the following equation as:

$$\rho = \left[\frac{E}{(1+\upsilon)}\right]\left(\frac{\partial \varepsilon}{\partial(\sin^2 \Psi)}\right) \tag{2}$$

where E is the elastic modulus, and υ is Poisson's ratio. The values of E and υ were measured by the ultrasonic reflection method. Plane (4 1 6) of the Al_2O_3 matrix was chosen to measure the residual stress due to its high diffraction angle and high diffraction intensity.

Table 2
Mechanical properties of the Cr_3C_2/Al_2O_3 nanocomposites

Deposition time (h)	Fracture strength (MPa)	Toughness (MPa m$^{1/2}$)
0 (monolithic Al_2O_3)	370	4.0
0.5	404	4.5
1	420	5.3
1.5	450	5.3
2	465	5.6

Table 3
Residual stresses of Al_2O_3 and nanocomposites prepared by MOCVD in fluidized bed and hot pressed

	Monolithic Al_2O_3	5.2 vol% Cr_3C_2/Al_2O_3	6.8 vol% Cr_3C_2/Al_2O_3
Young's modulus (GPa)	452	459	463
Poisson's ratio	0.41	0.44	0.48
Residual stress (MPa)	−84	−104	−125

3. Results and discussion

3.1. Microstructure characterization

The results of the apparent density and porosity of hot-pressed samples of chromium carbide/alumina composites sintered at 1500 °C for 1 h are listed in Table 1. The relative density of the monolithic Al_2O_3 sintered under identical conditions is 99.2%. The apparent density of the composites is found to increase with increasing deposition time and the porosity of all the composites is between 1–2 vol%. Inability to estimate the contents of the second phase due to limitations in resolution, inhibits the accurate estimation of the relative density of the composites. Its presence can be confirmed by SEM observation of the polished surface.

The FE-SEM micrographs of the sintered composite prepared by MOCVD for 2 h and hot-pressed at 1500 °C/1 h under vacuum are shown in Fig. 1. The brighter nanosized second phases are uniformly distributed at the grain boundary of the grey matrix. Since the atomic number of Cr is higher than Al, the brighter phase in the back-scattered contrast image is that of Cr-carbide while the grey phase comprises of Al_2O_3 matrix. (Fig. 1(b)) The pore-free morphology shows that the composite has achieved full density after hot-press sintering at 1500 °C. The average grain size of the second phase and of Al_2O_3 is 100 nm and 1.2 μm, respectively. The elemental analysis of the second phase by EDS (not shown here) confirms that the second phase contains Cr and C. The carbides as observed by SEM belong to the intergranular second phases.

Fig. 2 shows a representative TEM micrograph of the nanocomposite. The microstructure shows the dark spherical second phases dispersed uniformly inside the Al_2O_3 grains or at the grain boundary. In addition to the intergranular Cr-carbide found by SEM, the TEM image indicates presence of intergranular and intragranular Cr-carbides in the nanocomposite. Fig. 2(b) shows the diffraction pattern of the second phase (marked as B in Fig. 2) and is found to comprise of Cr_3C_2. It can be deciphered from the SEM micrograph that the intragranular Cr_3C_2 possesses smaller grain size, in the range 10–50 nm; as compared to the intergranular Cr_3C_2 grain size which falls in the submicron range. Therefore, we can conclude that the Cr_3C_2/Al_2O_3 nanocomposite prepared by MOCVD via fluidized bed is an intra/inter type of nanocomposite.[1]

From our previous investigations,[18] as-received powder from the MOCVD method in a fluidized bed comprised of a layer of amorphous Cr_2O_3 coated on the surface of Al_2O_3 powder. Therefore, in the initial stage of sintering, the Cr_2O_3 was located at the grain boundary of the matrix. Then the oxide carbonized to Cr_3C_2 at temperatures higher than 1200 °C.[19] In the final stage of sintering, the second phase was coarsened by the grain

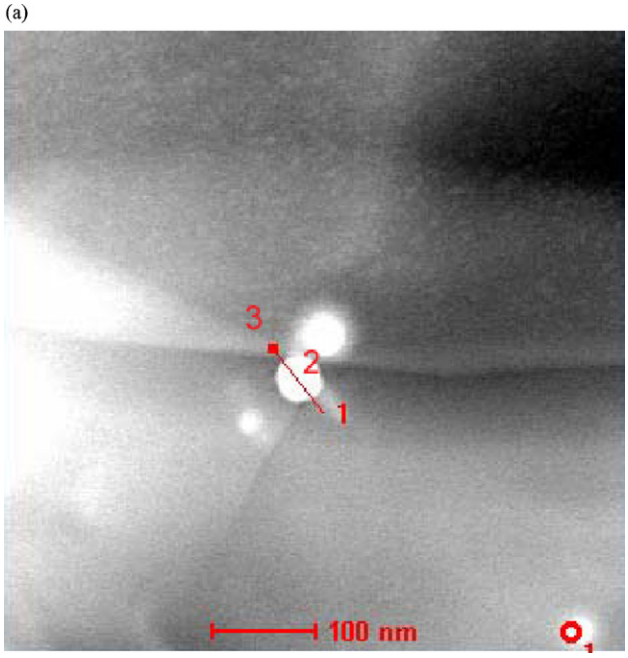

Fig. 4. HAADF analysis of chromium carbide/alumina nanocomposites prepared by MOCVD method for 2 h and hot-pressed at 1500 °C for 1 h in vacuum (a) image of analytical zone. (b) Line profile results; (c) EDS spectra of the relative line profile.

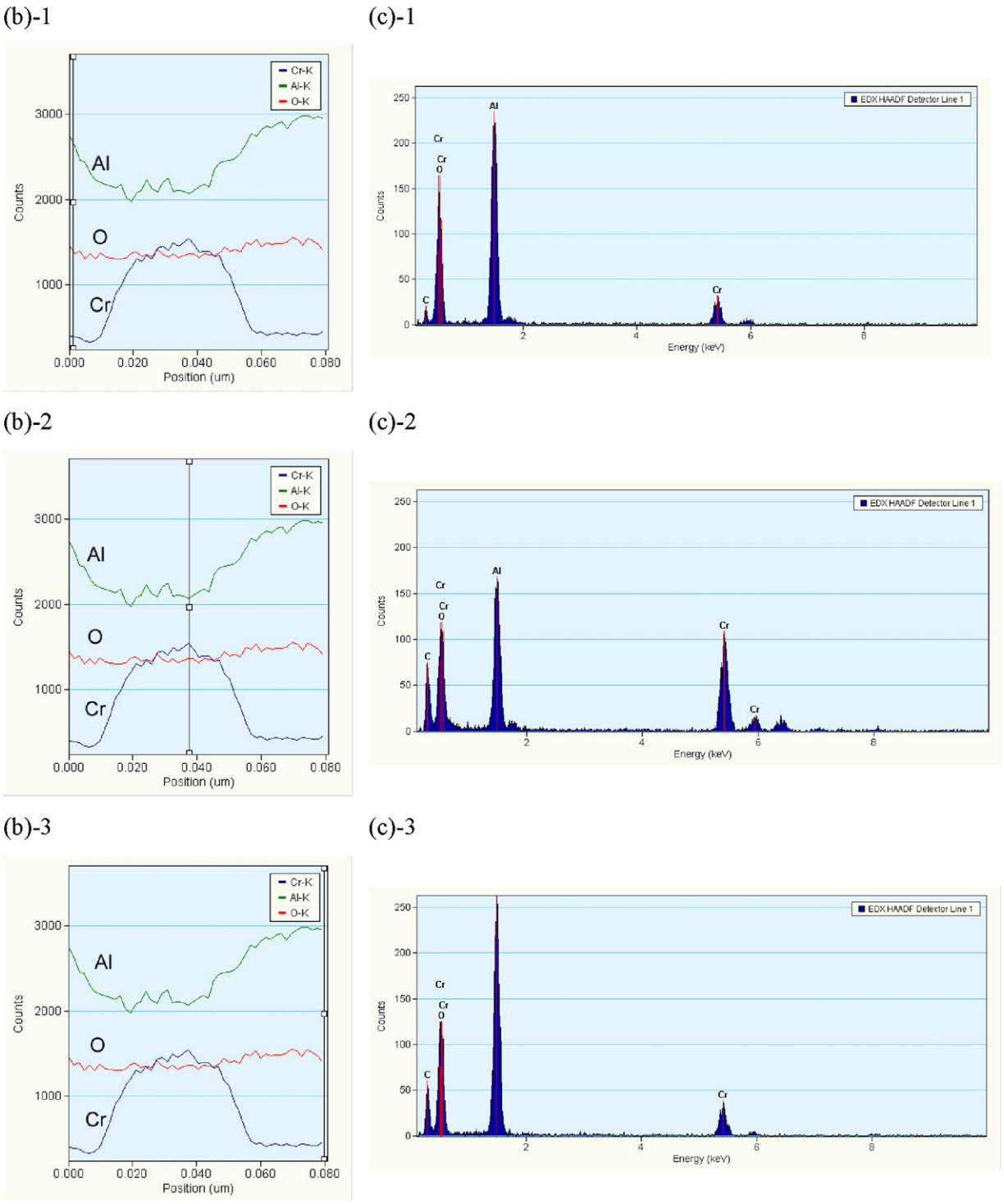

Fig. 4. (*Continued*).

growth of Al_2O_3, although some nanosized second phase was embedded in the grains of coalesced Al_2O_3. While the nanosized Cr_3C_2 phase was trapped inside the Al_2O_3 grain, the size of the carbide remained constant due to the lack of a diffusion path. In contrast, the intergranular Cr_3C_2 phases increased by several multiples due to the coalescence effect and the grain boundary diffusion path.

The chromium carbide contents with different deposition time are displayed in Table 1. The second phase volumes are estimated using Eq. (1) by taking this porosity into account. (The sample might also contain some closed porosity; so the values can even be higher.) The Cr_3C_2 content increases with increasing deposition time in the fluidized bed and reaches saturation after 1.5 h of deposition. A maximum of 6.8 vol% Cr_3C_2/Al_2O_3 nanocomposite can be prepared after 2 h of coating by MOCVD. According to the report of Lin et al. on Mo/Al_2O_3 composite,[20] the volume fraction of the second phase will influence the microstructure and the type of the nanocomposite. If the second

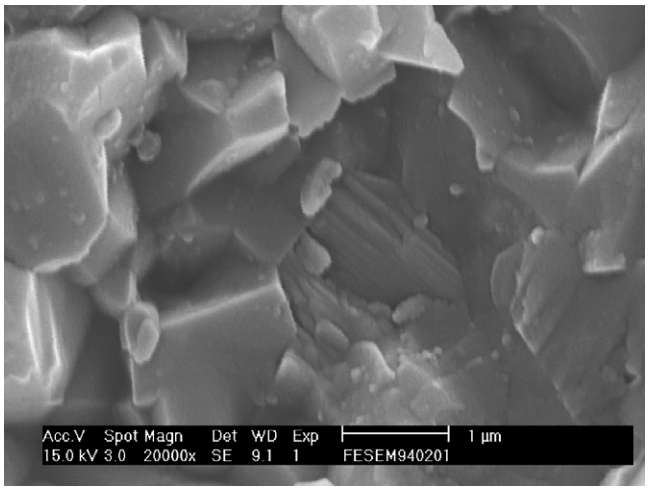

Fig. 5. FE-SEM micrograph on fracture surface of chromium carbide/alumina nanocomposites prepared by MOCVD method for 2 h and hot-pressed at 1500 °C for 1 h in vacuum.

phase content ranges from 1 to 4 vol%, the microstructure of the nanocomposite tends to evolve inter- and intragranular type, while the diameter for both locations is smaller than 100 nm. However, when the volume fraction of the second phase ranges from 5 to 15 vol%, the microstructure of the nanocomposite is related to the inter-submicron and intra-nano-granular type. The microstructural evolution of the Mo/Al_2O_3 nanocomposites is in co-ordination with the SEM and TEM results in this study. When the MOCVD coating time is 2 h, more Cr species have a high probability of coalescing as larger grains on the grain boundary of the matrix. As shown in Fig. 3, the Cr_3C_2 neighboring grains located at the triple junction of the Al_2O_3 matrix acquire larger grain size after further sintering. Some sessile dislocations are located around the vicinity of the second phase.

3.2. Mechanical properties of the Cr_3C_2/Al_2O_3 nanocomposite

Table 2 shows that the fracture strength and toughness of the Cr_3C_2/Al_2O_3 nanocomposite increases with increasing deposition time; albeit the fracture strength increases almost linearly with increasing contents of Cr_3C_2 phase. Comparing with the strength of monolithic Al_2O_3 (370 MPa), the 6.8 vol% Cr_3C_2/Al_2O_3 nanocomposite possesses the maximum fracture strength of 465 MPa which is a 20% improvement.

The toughness of monolithic Al_2O_3 prepared by the same procedure is 3.9 MPa $m^{1/2}$. As the second phase increases, the toughness increases and reaches its highest values after one hour of deposition and remains almost constant even after longer deposition times. The values of 5.6 MPa $m^{1/2}$ have 45% improvement over monolithic Al_2O_3.

The grain size of Al_2O_3 matrix in the 6.8 vol% Cr_3C_2/Al_2O_3 nanocomposite is 1.2 μm, which is smaller than the 1.3 μm value for monolithic Al_2O_3. The microstructural results show that the refinement of the Al_2O_3 by adding of the Cr_3C_2 phase is insignificant. Thus, the strengthening mechanisms in this system are proposed to be by the grain boundary strengthening mechanism and dislocation model[21] which are caused by inclusion of the solid solution of Cr_2O_3 in Al_2O_3 grain and residual stress caused by the mismatch of thermal expansion coefficients.

It is found that the characteristic color of the 2.2 vol% Cr_3C_2/Al_2O_3 nanocomposite transformed from white (that of the monolithic Al_2O_3) to pink. With further addition of Cr_3C_2, the characteristic color of the nanocomposite turned to black with a tint of pink. This color change is attributed to the solid solution formation, in which the Cr^{3+} ions are occupying part of the octahedral interstitial site of the Al^{3+} in the corundum structure, similar to the octahedral sites of the ruby structure.[22] The HAADF image of the Cr_3C_2/Al_2O_3 composite with a line profile and the EDS analysis results are shown in Fig. 4. A trace amount of the Cr spectrum was found in the Al_2O_3 matrix and its content seems to be increased at the grain boundary of the matrix (point 3). The incorporation of the Cr^{3+} ion causes an expansion of the octahedron and induces compressive residual stress, which strengthens the grain boundary. The grain boundary strengthening produces the change of the fracture mode.

The fracture strength of the grain boundary is usually lower than that within the grains. Hence, the monolithic Al_2O_3 ceramic exhibits a mainly intergranular fracture mode. However, the Cr_3C_2/Al_2O_3 nanocomposite changes to intergranular and transgranular fracture mixed mode, as shown in Fig. 5. The fracture surface of the nanocomposite shows the planar cleavage plane and step-wise fracture surface. Awaji et al.[23] suggest that the steps observed on the fracture surface can be evidence of the existence of nanocracking around the second phase particles.

Fig. 6 shows a TEM micrograph of Cr_3C_2/Al_2O_3 nanocomposite. Tangled dislocation can easily be found around the second phase. Choi et al.[21] proposed that the dislocation in ceramic nanocomposite releases tensile residual stresses in the

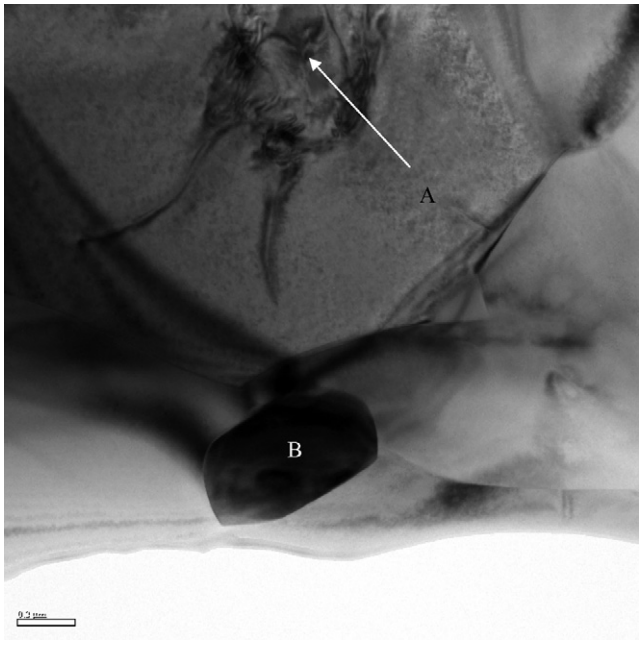

Fig. 6. TEM micrograph of chromium carbide/alumina nanocomposites prepared by MOCVD method for 2 h and hot-pressed at 1500 °C for 1 h in vacuum. (A) Dislocation tangled, (B) sub-micron intergranular Cr_3C_2.

matrix. Consequently, the defects size along the grain boundary is reduced. Thus, the dislocation reduces both the defect size along the grain boundaries and the tensile residual stresses in the matrix, resulting in improvement of the strength of the nanocomposite. Also, the sessile dislocation serves as epicentre of stress concentration, and creates small nanocracks[23] or wedge-like opening effect[24] in the vicinity of a main crack tip.

3.3. Residual stress

Fig. 7 shows the relationship of residual stress and the $\sin^2\psi$ of the monolithic Al_2O_3 and Cr_3C_2/Al_2O_3 nanocomposites. These results indicate that the residual compressive strain (negative slope) increases with increasing the content of Cr_3C_2 phase in the Al_2O_3 matrix. Thus, the residual stress can be determined by including the slope of the lines, the measured Young's modulus and the Poisson's ratio into Eq. (2). The calculated values are listed in Table 3. It is noted that the hot-pressed monolithic Al_2O_3 shows compressive residual stress of −81 MPa. It is believed that the compressive stress is due to the combined effects of the di-axial mechanical compress stress of hot-pressed sintering and the anisotropic thermal expansion of the Al_2O_3 grains. Hence, the residual stress of the 2.2 and 5 vol% Cr_3C_2/Al_2O_3 nanocomposites was subtracted from the residual stress of sintered Al_2O_3 stress. The net residual stress caused by the addition of the second phase and the solid solution for the 2.2 and 5 vol% Cr_3C_2/Al_2O_3 nanocomposites is −20 and −41 MPa, respectively.

As the thermal expansion coefficient of the Cr_3C_2 (1.12×10^{-5}/°C) is larger than the Al_2O_3 matrix (8.4×10^{-6}/°C), mismatch of the thermal coefficients creates the radial tensile stress and tangential compressive stress in the matrix around the second phase.[25] In addition, the solid solution of the Cr^{3+} atoms in solid solution imposes lattice strains on the surrounding host atoms. As shown in Fig. 8, the SEM micrograph of the crack deflection along the propagation direction of the nanocomposite. The transgranular cracking is deflected by the radial tensile stress field around

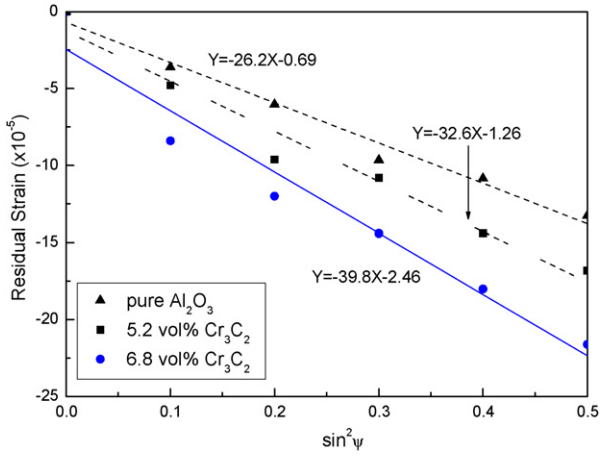

Fig. 7. Residual strains of Al_2O_3 and nanocomposites prepared by MOCVD in fluidized bed and hot pressed.

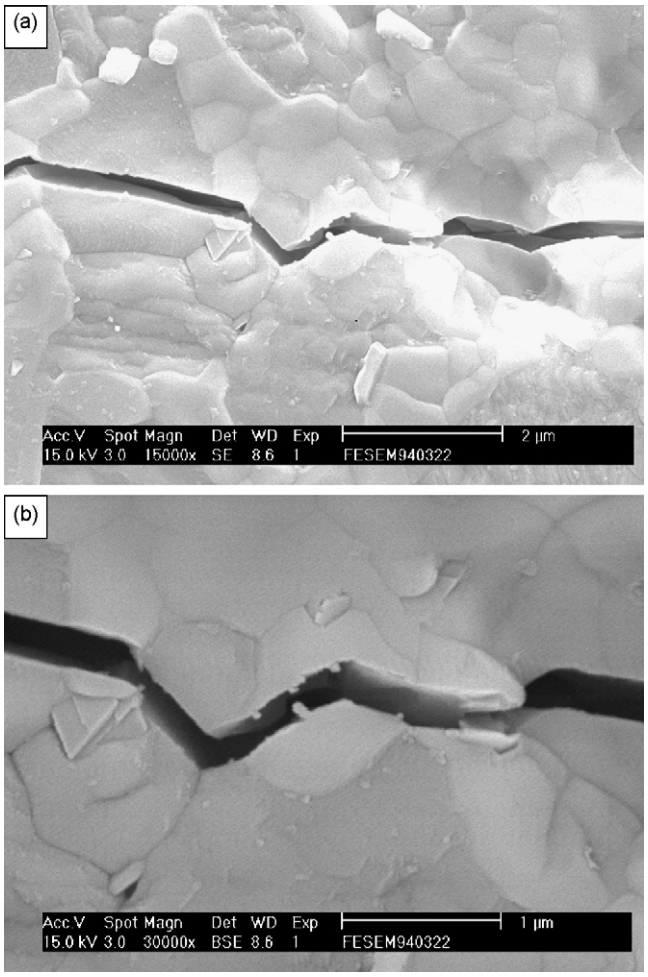

Fig. 8. FE-SEM micrographs of crack morphologies around the Vicker's indentation for chromium carbide/alumina nanocomposites. (a) Over view, and (b) close view.

the inclusions, while consumed the propagation energy by the compressive stress in the matrix and increased traveling distance during the crack extension. In addition, the toughness of the nanocomposite increases by the dual interaction of the crack front with the residual stress via the second phase and also with the lattice strain field via the impurity solid solution atoms. Therefore, this crack deflects and residual stress mechanism is suggested as the major toughening mechanism in Cr_3C_2/Al_2O_3 nanocomposite. Lastly, crack branching, and nano/micro-carck mechanism also can be found in this system and act as a minor mechanism.

4. Conclusions

Intra/inter type nanocomposite Cr_3C_2/Al_2O_3 can be fabricated by MOCVD (conducted in the fluidized bed) and hot-press sintering route. This followed by 1500 °C hot-pressed sintering for 1 h can fully consolidate the composites in the second phase ranging from 0 to 5 vol%. The intergranular and intragranular Cr_3C_2 grains with sizes of 100 nm and 30–50 nm, respectively, were well dispersed in the Al_2O_3 matrix. The addition of 6.8 vol% nanosized second phase strengthened

the Al_2O_3 matrix and improved the fracture strength from 370 MPa to 465 MPa while the toughness increased to 45% from that of monolithic Al_2O_3. The fracture mode changed from the intergranular (that of the monolithic Al_2O_3) to the intergranular–transgranular mixture mode of the nanocomposite caused by the residual stress. The magnitude of residual compressive stress produced by inclusion of the solid solution of the Cr^{3+} in the Al_2O_3 lattice concomitant with the mismatch of the thermal expansion coefficient of the second phase and matrix, is −20 and −41 MPa for the 5.2 and 6.8 vol% Cr_3C_2/Al_2O_3 nanocomposite, respectively. The toughening mechanism of the nanocomposite contributes to the crack deflection and the residual stress.

Acknowledgment

The authors would like to thank the National Science Council of Taiwan, Republic of China, for its final support under contract no. NSC 95-2221-E-218-018.

References

1. Niihara, K., New design concept of structural ceramics–ceramic nanocomposite. *J. Ceram. Soc. Jpn.*, 1991, **99**(10), 974–982.
2. Nawa, M., Sekino, T. and Niihara, K., Microstructure and mechanical properties of Al_2O_3-MO nanocomposites. *J. Jpn. Soc. Powd. Powd. Metal.*, 1992, **39**, 1104–1108.
3. Nakahira, A. and Niihara, K., Sintering behavior and consolidation process for Al_2O_3/SiC nanocomposites. *J. Ceram. Soc. Jpn.*, 1992, **100**(4), 448–453.
4. Fu, C. T. and Wu, J. M., Microstructure and mechanical properties of Cr_3C_2 particulate reinforced Al_2O_3 matrix composites. *J. Mater. Sci.*, 1994, **29**(10–13), 2617–2677.
5. Nakahira, A., Niihara, K., Ohkijima, J. and Hirai, T., The Al_2O_3/Si_3N_4 nano-composites. *J. Jpn. Soc. Powd. Powd. Metal.*, 1989, **36**, 239–242.
6. Inoue, S., Uchiyama, T. and Niihara, K., Al_2O_3/SiC whisker/ZrO_2 ceramics composite. *J. Jpn. Soc. Powd. Metal.*, 1990, **37**, 341.
7. Fu, C.-T. and Li, A.-K., Dependence of surface damage induced by electrical-discharge machining on the fracture strength of Al_2O_3-Cr_3C_2 composites. *Mater. Chem. Phys.*, 1994, **39**(2), 129–135.
8. Balachandran, U., Siegel, R. W., Liao, Y. X. and Askew, T. R., Synthesis, sintering, and magnetic properties of nanophase Cr_2O_3. *Nanostruct. Mater.*, 1995, **5**, 505–512.
9. Peters, G., Jerg, K. and Schramm, B., Characterization of chromium (III) oxide powders prepared by laser-induced pyrolysis of chromyl chloride. *Mater. Chem. Phys.*, 1998, **55**, 197–201.
10. Chatterjee, M., Siladitya, B. and Ganguli, D., Chromia microspheres by the sol–gel technique. *Mater. Lett.*, 1995, **25**(25), 261–263.
11. Kawabata, A., Yoshinaka, M., Hirota, K. and Yamaguchi, O., Hot isostatic pressing and characterization of sol–gel-derived chromium(III) oxide. *J. Am. Ceram. Soc.*, 1995, **78**(8), 2271–2273.
12. Vollath, D., Szabo, D. V. and Willis, J. O., Magnetic properties of nanocrystalline Cr_2O_3 synthesized in a microwave plasma. *Mater. Lett.*, 1996, **29**, 271–279.
13. Zhu, Y., Qian, Y. and Zhang, M., γ-Radiation synthesis of nanometer-size amorphous Cr_2O_3 powders at room temperature. *Mater. Sci. Eng.*, 1996, **B41**, 294–296.
14. Lin, H.-T., Huang, W.-S., Wang, S.-C., Lu, H.-H., Wei, W.-C. J. and Huang, J.-L., *Mater. Sci. Eng. B*, 2006, **127**, 22–28.
15. Rice, R. W., Toughening in ceramics particulate and whisker composites. *Ceram. Eng. Sci. Proc.*, 1990, **11**(7–8), 667–694.
16. JCPDS, PDF number: 035-0804.
17. Cullity, B. D. and Stock, S. R., Elements of X-ray diffraction. *Chap. 15 Stress Measurement*. Prentice Hall, NJ, 2001, pp. 435–469.
18. Lin, H.-T., Wang, S.-C., Huang, J.-L., Chang, S. Y. *et al.*, Processing of hot-pressed Al_2O_3–Cr_2O_3/Cr-carbide nanocomposite prepared by MOCVD in fluidized bed. *J. Eur. Ceram. Soc.*, 2007, **27**, 4759–4765.
19. Rajagopalan, P. K., Krishnan, T. S. and Bose, D. K., Development of carbothermy for the preparation of hepta chromium carbide. *J. Alloys Compounds*, 2000, **297**, L1–L4.
20. Lin, C.-J., Yang, C.-C. and Wei, W.-C. J., Processing and microstructure of nano-Mo/Al_2O_3 composites from MOCVD and fluidized bed. *NanoStruct. Mater.*, 1999, **11**(8), 1361–1377.
21. Choi, S. M. and Awaji, H., Nanocomposites—a new material design concept. *Sci. Technol. Adv. Mater.*, 2005, **6**, 2–10.
22. Pokorny, P. and Ibarra, A., Impurity effects on the thermoluminescence of Al_2O_3. *J. Appl. Phys.*, 1994, **75**(2), 1088–1092.
23. Awaji, H., Choi, S.-J. and Yage, E., Mechanisms of toughening and strengthening in ceramics-based nanocomposites. *Mech. Mater.*, 2002, **34**, 411–422.
24. Pezzotti, G. and Muller, W. H., Strengthening mechanisms in Al_2O_3/SiC nanocomposites. *Comput. Mater. Sci.*, 2001, **22**, 155–168.
25. Chwala, K. K., *Ceramic Matrix Composites*. Chapman & Hall, London, 1993 [Chap. 8, pp. 274–290].